DEVELOPMENT OF A TISSUE-ENGINEERED EYE MODEL TO TEST DRUG DELIVERY SYSTEMS

By

KATIE OSWALT

Bachelor of Science in Chemical and Biological Engineering

University of Colorado Boulder

Boulder, Colorado

2018

Submitted to the Faculty of the
Graduate College of the
Oklahoma State University
in partial fulfillment of
the requirements for
the Degree of
MASTER OF SCIENCE
December 2021

DEVELOPMENT OF A TISSUE-ENGINEERED EYE MODEL TO TEST DRUG DELIVERY SYSTEMS

Thesis Approved:

Dr. Heather Fahlenkamp

Thesis Adviser

Dr. Josh Ramsey

Dr. Craig Miller

ACKNOWLEDGEMENTS

Parts of this work were carried out in the Microscopy Laboratory, Oklahoma State University, which received funds for purchasing the equipment from the NSF MRI program. I would like to thank Lisa Whitworth and Brent Johnson for their help using the instruments at the OSU Microscopy Laboratory. I would like to thank Dr. Gibran Ali for his help when developing my immunochemical staining procedure. I would like to thank Dr. Lin Liu and Dr. Yurong Liang for helping perform PCR analysis for my samples. I would also like to thank Dr. Josh Ramsey and Dr. Craig Miller for serving as members of my advisory committee. Finally, I would like to thank Dr. Heather Fahlenkamp for her guidance as my research advisor during this project.

Name: KATIE OSWALT

Date of Degree: DECEMBER 2021

Title of Study: DEVELOPMENT OF A TISSUE-ENGINEERED EYE MODEL TO TEST DRUG DELIVERY SYSTEMS

Major Field: CHEMICAL ENGINEERING

Abstract:

One of the leading causes of blindness is diabetic retinopathy, a disease that affects the posterior segment of the eye. Injections are commonly used to treat diabetic retinopathy, but they can lead to discomfort and low patient compliance. Animal models are the current standard when obtaining preclinical data for new treatment options, but current research aims to create in vitro models that can reduce or replace the use of animal models. Therefore, the goal of this project was to develop a three-dimensional tissue model that can be used to test drug delivery systems created for the treatment of posterior eye diseases. Our model consists of two-modules that, when paired together, can replicate drug transport through the cornea and the interaction between the drug and the retinal endothelium. The first module represents the corneal epithelium, the main barrier of drug transport of the eye. The second module represents the vitreous humor and the retinal endothelium, the target cell layer for treatment of diabetic retinopathy.

Results of this project show that we were able to establish a corneal epithelium and a retinal endothelium of human primary cells within each module. The corneal epithelium had 3-4 cell layers, showed cytokeratin-3 expression, but lacked expression of zonula occludens-1, a tight junction protein present in the cornea in vivo. The epithelium provided a barrier to paracellular transport, but permeability coefficients and transepithelial electrical resistance (TEER) values indicated the model had a weaker barrier after culturing at air-liquid interface when compared to remaining in submerged culture conditions. The retinal endothelium expressed both VCAM-1 and ICAM-1, cellular markers characteristic of activation, after exposure to TNF-α, a proinflammatory cytokine. Gene expression and secretion of inflammatory cytokines from the retinal endothelial cells were also significantly increased in response to TNF-α. Overall, we show that the cornea module provides a barrier to drug transport, and the retina module provides a retinal endothelium that can be activated in response to inflammation, similar to that expected in diabetic retinopathy.

TABLE OF CONTENTS

Chapter **Page**

Chapter **Page**

LIST OF TABLES

Table **Page**

LIST OF FIGURES

Figure **Page**

CHAPTER I

INTRODUCTION

The most recent statistics from 2020 estimate that 43.3 million people worldwide are blind [3]. The main causes of blindness are diabetic retinopathy, glaucoma, macular degeneration, cataracts, and refractive errors [3]. Diabetic retinopathy, glaucoma, and macular degeneration affect the posterior segment of the eye. Treatment options for posterior eye diseases include diet modifications, surgery or laser therapy, or pharmacotherapy. Diet modifications typically focus on regulating or maintaining macro- and micronutrients, such as blood sugar and vitamins [4, 5]. However, diet modifications are only a preventative treatment option and do not have much impact in the treatment of the disease. Surgery and laser therapy try to correct the damage caused by the underlying disease. Common practices include removing excess fluid in the eye, creating areas for fluid drainage, or sealing off leaking blood vessels [4-6]. Pharmacotherapy is used to treat the retinal disease, and the most common forms of pharmacotherapy are eye drops and injections [4-6]. Eye drops are not very effective for treating retinal diseases because the short contact time on the cornea limits drug absorption, and injections may be uncomfortable for patients and must be performed by trained personnel. Other ocular drug delivery methods include gels and creams, which have similar drawbacks as eye drops, and ocular inserts, which also requires trained personnel for application.

Alternate drug formulations and routes of administration for treatment of posterior eye diseases are being considered and have been reviewed [7, 8]. Our lab has developed a minimally

invasive drug delivery system that aims to deliver drugs to the retina at therapeutic levels for an extended period of time. The delivery system is composed of nanoparticles encapsulating a drug which are then embedded in a collagen membrane. This membrane can then be paired with a contact lens to enable sustained delivery. The nanoparticle membranes have been previously tested under *in vitro* conditions [9]. The membranes had similar light transmittance to that of commercial contact lenses, and the drug release from the nanoparticles is more controlled when embedded in the collagen membranes.

The process for new drug delivery methods to move from a research lab to commercial availability relies heavily on animal models. Even though this is the accepted standard, an animal response can be different from humans, and if using excised animal tissues, there can be high variability due to how the tissues were handled and stored. Also, animal studies are expensive, and they raise the question of whether they are ethical. For these reasons, there is a push to reduce, refine, and replace the use of animal models in research. Therefore, there is a need to develop *in vitro* models that can accurately represent the biological system and predict *in vivo* behavior.

The overall goal of this project is to develop an *in vitro*, three-dimensional tissue model that can be used to test drug delivery systems for posterior eye diseases, specifically diabetic retinopathy. To achieve this goal, a two-module system was designed that contains a cornea module to mimic the barrier function of the eye and a retina module to mimic drug delivery through the vitreous humor to the retina. The cornea module is composed of human corneal epithelial cell (HCEC) layers which represent the corneal epithelium, the main barrier for drug delivery to the posterior segment of the eye. The retina module is composed of a collagen-hyaluronic acid (HA) gel, which represents the vitreous humor, and human retinal microvascular endothelial cells (HRMECs), which represents the vascular system of the retina. The first aim of this project is to create a cornea module that mimics the *in vivo* corneal epithelium by showing similar morphology, protein expression, and barrier functionality. The second aim of this project is to show HRMECs

cultured *in vitro* can be induced to an activated state to test the effect of anti-inflammatory drugs. Together, these modules can be used to test the transport of drugs through the cornea to the posterior part of the eye and the effect the drug on the retina.

CHAPTER II

BACKGROUND

2.1 Anatomy of the Eye

The eye can be divided into two distinct segments: (1) the anterior segment and (2) the posterior segment. As shown in Figure 1a, the anterior segment includes the cornea, pupil, iris, and lens, and the posterior segment includes the vitreous humor, retina, and optic nerve.

The cornea consists of three distinct layers – the epithelium, the stroma, and the endothelium (Fig. 1b). The first layer of the cornea is the corneal epithelium. It is a stratified squamous epithelium composed of 5-7 layers of cells [10]. The top 2-3 layers are superficial cells and have tight junctions between neighboring cells [10]. The tight junctions form a barrier to prevent paracellular transport of molecules through the corneal epithelium. On the posterior side of the epithelium is Bowman's layer. This layer is acellular, and its function is unknown, although there have been several ideas of its purpose [10, 11].

The second layer of the cornea is the stroma, which accounts for approximately 90% of the cornea thickness [12]. It is composed of carefully aligned collagen fibers and an extracellular matrix (ECM) that contribute to the transparency of the cornea. The collagen fibers are organized into parallel bundles to form lamellae, and multiple lamellae are layered at right angles to each other to form the stroma [10]. Keratocytes are found throughout the stroma and are responsible for producing and maintaining the collagen and ECM that forms the stroma. Descemet's membrane is

found on the posterior side of the stroma. The membrane is acellular and acts as the basement membrane for the endothelial cell layer of the cornea [13].

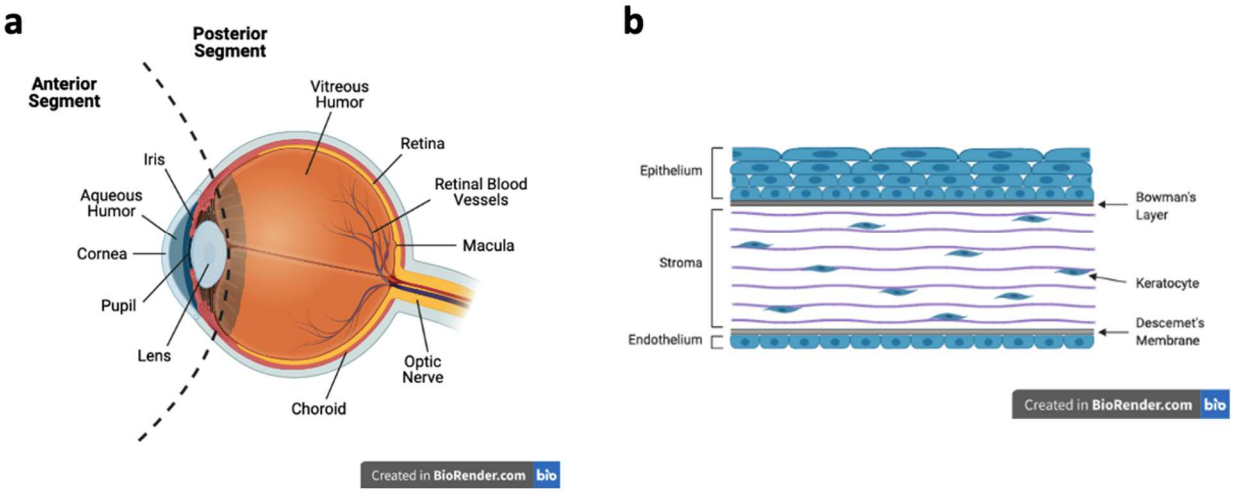

Figure 1. Anatomy of the eye (a) and organization of the cornea (b). Created with BioRender.com.

The corneal endothelium is found on the posterior side of Descemet's membrane and is the third and innermost layer of the cornea. It is a monolayer of hexagonal-shaped cells that contain Na^+K^+ATPase pumps [10], which are used to regulate ion movement across the cell layer. In addition to the structure of the stroma, the clarity of the cornea is a result of an active net flux of ions out of the stroma and into the aqueous humor due to these pumps [10, 12].

The anterior and posterior segments of the eye are directly adjacent to each other. The transition between the two segments occurs at the interface of the lens and the vitreous humor. The vitreous humor is avascular and accounts for two-thirds of the volume of the eye [12]. It is composed mainly of water, but also contains collagen and hyaluronic acid, which gives it a gel-like consistency [12].

The retina surrounds the vitreous humor and extends from the optic nerve towards the anterior segment of the eye. The retina is composed of several cellular layers including neural cells and photoreceptor cells [12, 14]. The outermost cell layer of the retina is the retinal pigment

epithelium (RPE). RPE cells have multiple functions including light absorption and active transport of materials into and out of the retina [12]. Moving inward from the retinal pigment epithelium, the next several cell layers contain the nerve cell bodies (nuclear layers) and synapses (plexiform layers) of the retina. The structure of these layers can be seen in Figure 2. The outer nuclear layer contains the photoreceptor cells, which are comprised of both rods and cones and are responsible for detecting color in vision [14]. The inner nuclear layer contains multiple cell types, but are classified as either horizontal, bipolar, or amacrine cells [2, 12]. The last nerve cell layer contains the ganglion cells. The nerve cells of each layer are connected to each other through synaptic interactions within the plexiform layers. The synaptic signals from the first two nerve layers are collected in the inner plexiform layer, and the ganglion cell layer sends the accumulated information to the brain though the optic nerve [2, 14]. The macular region of the retina contains the fovea. This area of the retina has only cone photoreceptors and are at their highest density in this region [12]. The fovea is responsible for visual acuity and color vision, and damage to the fovea can result in blindness [2, 12, 14].

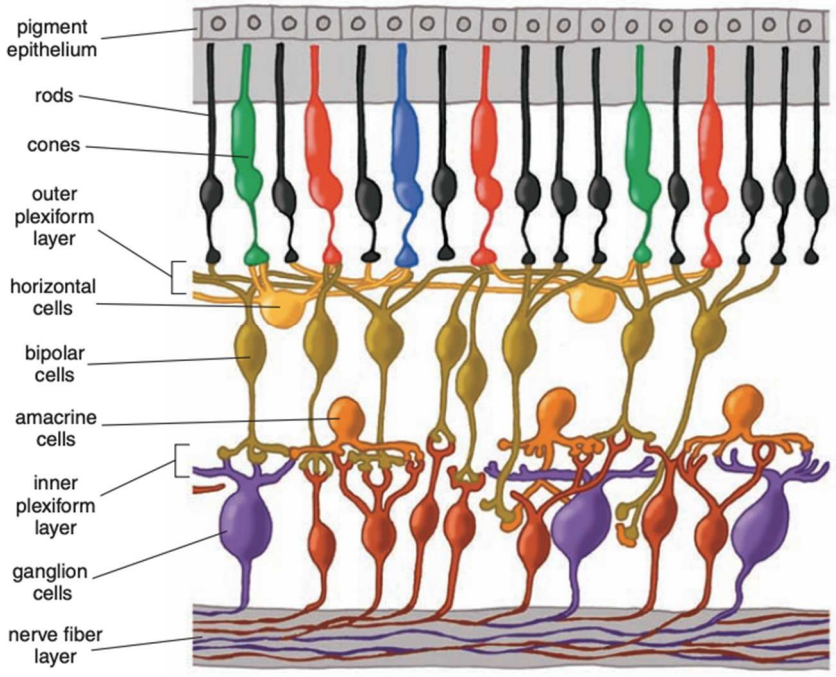

Figure 2. Organization of the retina. Adapted from [2].

The retina receives its blood supply from two sources: (1) the choroidal blood vessels and (2) the central retinal artery. The RPE and the photoreceptors receive blood from the choroidal blood vessels, and the remainder of the retinal layers receive their blood supply from vessels of the central retinal artery, which stems from the optic nerve [12, 14]. The fovea, however, is avascular. Retinal blood vessels form a ring around the fovea, and the only supply of blood to the fovea comes from the choroidal blood vessels [12]. Tight junctions between the RPE cells form the outer blood-retinal barrier between the choroid and the outer layers of the retina, while nonfenestrated endothelial cells of the retinal blood vessels form the inner blood-retinal barrier for the inner layers of the retina [12].

2.2 Posterior Eye Diseases and Treatments

As previously mentioned, the most common causes of blindness are macular degeneration, glaucoma, diabetic retinopathy, cataracts, and refractive errors. Macular degeneration, glaucoma, and diabetic retinopathy all effect the posterior segment of the eye.

Macular degeneration, or age-related macular degeneration (AMD), occurs when the macula becomes damaged. Since this area is responsible for visual acuity, damage to the fovea results in loss of central vision [15]. AMD can be classified as either “dry” or “wet” AMD. Dry AMD is the main type of AMD seen, and results as the macula thins with age and develops deposits of lipids underneath the RPE called drusen [15-17]. Although the mechanism is unknown, it is thought that dry AMD will progress to wet AMD, which is characterized by excess fluid in the retina and choroidal neovascularization [15-17]. There are no treatments for dry AMD, but disease progression may be slowed with a diet high in certain vitamins and minerals [5, 15, 16]. Wet AMD can be treated by laser photocoagulation to seal leaking blood vessels or intravitreal injections of anti-vascular endothelial growth factor (VEGF) drugs [5, 15, 16].

Glaucoma is a condition that can arise from an increase in intraocular pressure. Due to fluid accumulation within the vitreous humor, the optic nerve and retinal ganglion cells experience a higher-than-normal pressure, which causes the death of these cells after prolonged exposure [6, 18, 19]. Eye drops to lower intraocular eye pressure are typically used to treat glaucoma, but surgical procedures to create paths for fluid drainage can also be used [6, 18, 19].

The focus of this project is the treatment of diabetic retinopathy. As such, this disease and its current treatment options are discussed in more detail below.

2.2.1 Diabetic Retinopathy and Inflammation

There are two types of diabetic retinopathy (DR) – nonproliferative diabetic retinopathy (NPDR) and proliferative diabetic retinopathy (PDR). NPDR can be classified by its severity, ranging from mild to severe [1, 20, 21]. As NPDR becomes more severe, it can progress to PDR. Characteristics of NPDR include aneurysms, hemorrhages, and irregularities in the retinal microvasculature [20]. Once neovascularization is observed, the disease is classified as PDR [20]. Treatment options and disease prognosis for patients are better the earlier DR is diagnosed [20]. Diabetic macular edema (DME) is a condition that can develop at any point of DR [1, 21]. DME is caused by accumulation of fluid in the retina due to a leaking vasculature system and is characterized by thickening of the retina near the macula [1, 20, 21].

The pathways underlying development of DR are believed to be triggered by hyperglycemia, which is characteristic of diabetes (Fig. 3). One such mechanism of increasing interest is inflammation. Increased leukostasis, an inflammatory response, occurs in diabetic animal models [22-24], and it has been shown that the binding of leukocytes to retinal endothelial cells causes cell injury and eventually cell death in rodents [22, 25]. Because of the many similarities between diabetes in humans and rats, it is believed that leukocyte binding also causes retinal endothelial cell death in humans. Endothelial cell death occurs because leukocyte binding in the

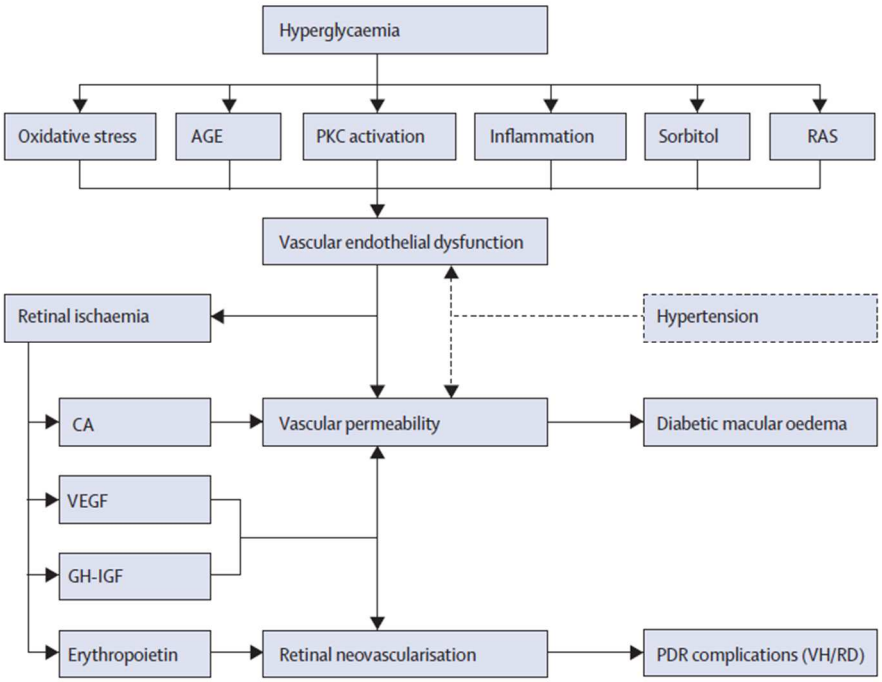

Figure 3. Pathophysiology of diabetic retinopathy. Adapted from [1]. AGE: advanced glycation end-products. PKC: protein kinase C. RAS: renin-angiotensin system. CA: carbonic anhydrase. VEGF: vascular endothelial growth factor. GH-IGF: growth factor-insulin growth factor. PDR: proliferative diabetic retinopathy. VH: vitreous hemorrhage. RD: retinal detachment.

vessels of the retina can decrease or stop blood flow. Downstream of the blockage, these regions become ischemic, and endothelial cell death leaves acellular capillaries in the retina. When ischemia develops in the regions of the acellular capillaries, VEGF is upregulated in response to promote neovascularization to regain blood prefusion to the area, which causes the transition from NPDR to PDR [26, 27]. The clinical signs characteristic of DR result from retinal ischemia [28]. Ischemia can also lead to hypoxia, which is used as a retinal neovascularization model [29, 30]. Activated microglial cells in the retina release TNF-α [29], and angiogenesis results from secondary cytokines and growth factors that are produced in response to TNF-α [31].

However, *in vitro* models of DR using HRMECs are not responsive to high levels of glucose [32-34]. As a result, *in vitro* models use pathways, such as inflammation, that are initiated

by hyperglycemia to model DR. Proinflammatory cytokines, such as TNF-α and IL-1β, are present at elevated levels in people with DR [35-37], and as such, are used to mimic inflammation *in vitro* [32, 36-39]. TNF-α and IL-1β induce expression of other inflammatory cytokines, such as IL-6 and IL-8, in endothelial cells. IL-6 is the primary mediator of the first step in inflammation (the acute-phase response) and lymphocyte activation [40-43]. IL-8 is responsible for recruitment and activation of neutrophils [41, 44]. Increased expression of these cytokines in the retina initiates an inflammatory response by recruiting lymphocytes and neutrophils, both of which are types of leukocytes with roles in an immune response. Other effects of TNF-α and IL-1β include induction of procoagulant activity and increased transendothelial migration of leukocytes [45-47]. Increased procoagulant activity in endothelial cells may worsen vessel blockage that leads to ischemia in the retina. Also, increased leukocyte migration due to TNF-α and IL-1β paired with increased leukocyte recruitment due to IL-6 and IL-8 likely contributes to the leaking blood vessels seen in DR.

2.2.2 Treatment Options

Current treatments for DR range from preventative measures to surgical intervention. Preventative measures are intended to prevent or inhibit the progression of diabetic retinopathy. This is typically done by controlling blood sugar and blood pressure [1, 34]. Vitrectomy or retinal laser photocoagulation are used when surgical intervention is deemed necessary. Vitrectomy is not used exclusively for the treatment of DR but is a common treatment option. When undergoing vitrectomy for DR, cloudy areas of the vitreous and scarred areas of the retina are removed from the eye [48]. Vitrectomy is useful for reducing the risk of retinal neovascularization and developing DME, but it can also cause cataracts to form and neovascularization of the iris [1, 20, 34]. Laser photocoagulation is considered the gold standard for treating PDR and can also be used to treat DME [1]. The laser is used to destroy the hypoxic regions of the retina, excluding the macula, to prevent neovascularization [20]. This technology is effective in preventing more visual loss from

occurring, but it is uncommon to see the reversal of vision already lost. Side effects often seen with this technology include peripheral vision loss, reduced visual acuity, and night blindness [1, 20].

Corticosteroids are currently being used to treat DME. These anti-inflammatory medicines can either be injected into the eye or formulated as an implant that offers prolonged release of the drug [20]. This treatment is not usually the primary method and is used in combination with surgery or laser therapy that treats DR, the underlying cause of DME. However, the shift towards considering DR as an inflammatory disease may expand the use of anti-inflammatory drugs for treating DR in the future.

Research and clinical trials for alternative treatments options for DR are ongoing. Some of the more popular alternatives include intravitreal injections of anti-VEGF agents and corticosteroids [49, 50].

2.3 Ocular Tissue Models

2.3.1 Cornea Models

The intended use of most tissue-engineered cornea models is graft implantation to reduce the shortage of donor corneas. Due to this focus, most studies focus on model transparency and integration capability with the native cell populations. However, when designing a model for use in testing drug delivery systems, it is important to consider the functionality of the epithelial layer, specifically the barrier properties. Cornea models designed for drug transport are composed of corneal epithelial cells and are cultured on permeable membrane cell culture inserts to allow culturing at air-liquid interface (ALI) conditions. ALI is used when culturing corneal epithelial models because it helps promote the formation of the stratified squamous epithelium seen *in vivo* [51-53].

Most *in vitro* models use HCE-T cells [51, 54-58], an immortalized human corneal epithelial cell line, because they have well-defined characteristics [59]. However, models containing these cells have been stated to have a high variability in barrier phenotype [54], which can be seen in the wide range of reported transepithelial electrical resistances [51, 55-58]. Some have tried to standardize the procedure to make HCE-T models [57, 60], while others have attempted to identify factors causing variability [54]. Additionally, there have recently been some studies focused on developing models composed of human primary cells to avoid the drawbacks from using immortalized cells [61, 62]. These models using primary cells have less variability than *in vitro* models using cell lines, but there are no *in vitro* models that represent the entire drug delivery process from drug administration to therapeutic action.

2.3.2 Retina Models

Tissue-engineered retina models are often used to study disease progression and identify potential targets for treatment of these diseases. Models created to study diabetic retinopathy model the inner blood retinal barrier. Some models are a co-culture composed of endothelial cells and pericytes, and other models include glial cells to form a triple culture. Because these models use high glucose and hypoxic conditions to mimic diabetic conditions that promote DR, glial cells are essential in these models since proinflammatory cytokines are released from this cell type [63]. High glucose culture conditions promoted an increase in proinflammatory and oxidative stress mediators in glial cells and decreased barrier integrity in endothelial cells [64]. Under hypoxic conditions, increased expression of adhesion molecules in HRMECs and pericytes has been reported [65], and barrier properties of endothelial cells within a triple culture were shown to deteriorate [63]. *In vitro* disease models containing more than one cell type are often used because the cellular interactions are being studied; however, increasing the complexity of the model may not always show a more accurate representation of the *in vivo* environment. One study showed a co-culture of endothelial cells and pericytes under hypoxic and hyperglycemic culture conditions

exhibited increased pericyte viability and increased endothelial barrier integrity [66], which is opposite of what occurs *in vivo*. Although these models represent the diseased retina, their main focus is on understanding the factors involved in the blood-retinal barrier disruption.

CHAPTER III

MATERIALS AND METHODS

3.1 Reagents and Antibodies

Human corneal epithelial cells and the EpiGRO Human Ocular Epithelia Complete Media Kit were purchased from MilliporeSigma (Burlington, MA). Primary human retinal microvascular endothelial cells, Complete Classic Medium with serum and CultureBoost, Bac-Off Antibiotic, and Attachment Factor were purchased from Cell Systems (Kirkland, WA). Human fibronectin (Gibco), Medium 199 (10X) (Gibco), goat serum (Gibco), and Hoechst 33342 solution were purchased from Fisher Scientific (Waltham, MA). Type I bovine collagen solution was purchased from Advanced BioMatrix (San Diego, CA). Recombinant human TNF-α and high molecular weight hyaluronan were purchased from R&D Systems (Minneapolis, MN).

Mouse monoclonal anti-cytokeratin 3/2p (1:50 dilution, sc-80000) and rat monoclonal anti-ZO-1 (1:50 dilution, sc-33725) antibodies were purchased from Santa Cruz Biotechnology (Santa Cruz, CA). Purified mouse IgG1 κ isotype control (401402), purified rat IgG2a κ isotype control (400502), Alexa Fluor 594 goat anti-mouse IgG (1:100 dilution, 405326), Alexa Fluor 594 goat anti-rat IgG (1:100 dilution, 405422) were purchased from BioLegend (San Diego, CA). Mouse monoclonal anti-CD31 (1:500 dilution, ab9498), mouse monoclonal anti-ICAM1 (1:100 dilution, ab2213), mouse monoclonal anti-VCAM1 (1:100 dilution, ab212937), mouse IgG2a κ isotype control (ab18415), mouse IgG1 κ isotype control (ab170190), Alexa Fluor 488 goat anti-mouse

IgG (1:100 dilution, ab150113), and Alexa Fluor 594 goat anti-mouse IgG (1:200 dilution, ab150116) antibodies were purchased from Abcam (Cambridge, MA).

3.2 Cell Culture

HCECs received from MilliporeSigma were expanded in T-75 flasks coated with a fibronectin solution (25 μg/mL). HCECs were cultured in EpiGRO Human Ocular Epithelia Complete Media. Cells were passaged using Accutase (Fisher Scientific) once reaching 80-90% confluency. Cells were cryopreserved in Cryo-SFM (PromoCell; Heidelberg, Germany) and kept in liquid nitrogen storage. HCECs were added to the cornea module directly from liquid nitrogen storage.

HRMECs received from Cell Systems were expanded in T-75 flasks coated with Attachment Factor. HRMECs were cultured in Complete Classic Media supplemented with Bac-Off Antibiotic. Cells were passaged using Passage Reagent Group (Cell Systems) once reaching 80-90% confluency. Cells were cryopreserved in Cell Freezing Medium (Cell Systems) and kept in liquid nitrogen storage. HRMECs were added to the retina module from a proliferating culture.

3.2.1 Cornea Module

The cornea module is shown in Figure 4a. Permeable cell culture inserts (8.0 μm pore; CellTreat; Pepperell, MA) from a 24-well plate were coated with a fibronectin solution (25 μg/mL) for a minimum of 90 minutes. HCECs at passage 4 were seeded on the permeable inserts at a seeding density of 25,000 cells/cm^2. The models were cultured in EpiGRO media at 37°C and 5% CO_2. The submerged-ALI models were cultured submerged in media for seven days followed by culture at ALI for seven days. The submerged models were cultured submerged in media for fourteen days.

3.2.2 Retina Module

The retina module is shown in Figure 4b. Collagen-HA hydrogels were prepared by mixing 51.9% (v/v) type I bovine collagen (3.0 mg/mL), 6.49% (v/v) 10X Medium 199, 32.5% (v/v) 0.1 N sodium hydroxide, and 9.09% (v/v) hyaluronan gel (10 mg/mL). This solution was added to permeable inserts from a 24-well plate and incubated at 37°C for 45 minutes to form the hydrogels. Prior to seeding the HRMECs, the inserts were inverted and coated with Attachment Factor according to the manufacturer's instructions. HREMCs at passage 7 were seeded on the bottom surface of the permeable inserts at a seeding density of 20,000 cells/cm^2, and the inserts were incubated at 37°C and 5% CO_2. After 4 hours to allow cell attachment, the permeable inserts were returned upright to a 24-well plate containing Complete Classic media. The models were cultured in Complete Classic media at 37°C and 5% CO_2 until confluent (approximately 7 days) before activation with TNF-α (10 ng/mL in Complete Classic media).

3.2.3 Complete Eye Model

The complete model will be used to test drug transport through the corneal epithelium and collagen-HA gel and measure the effect of the transported drug on the retinal endothelium. First, nanoparticle transport from a nanoparticle-embedded collagen membrane through the corneal

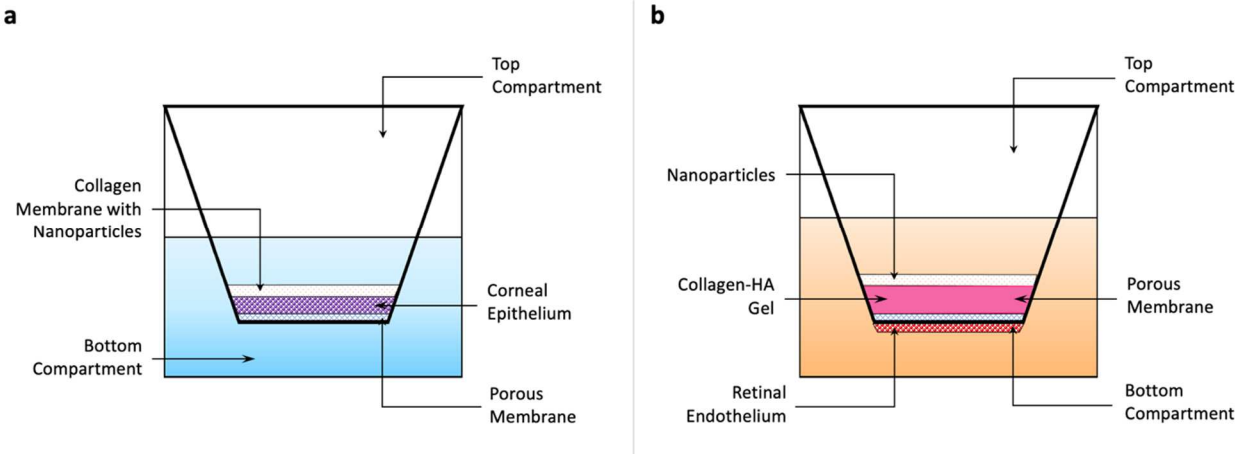

Figure 4. Diagram of the cornea (a) and retina (b) modules of the two-module engineered eye model.

epithelium will be measured in the cornea module (Fig. 4a). Then, using the transport data from the cornea module, nanoparticles in solution will be added to the retina module to and the interaction between the transported drug and the retinal endothelium can be measured (Fig. 4b).

3.3 Characterization of HCECs

3.3.1 Immunocytochemistry

To determine expression of cytokeratin-3 (CK3) and zonula occludens-1 (ZO-1), cells were fixed and permeabilized with BD Cytofix/Cytoperm solution (BD Biosciences; Franklin Lakes, NJ) for 20 minutes at 4°C. Cells were then blocked with 10% (v/v) goat serum and 1% bovine serum albumin (BSA) (MilliporeSigma; Burlington, MA) in Dulbecco's phosphate-buffered saline (DPBS) for 30 minutes at room temperature. Cells were incubated with the primary or isotype control antibodies diluted in 1% BSA and 0.1% (v/v) Tween-20 in DPBS overnight at 4°C in a humid chamber. Specific secondary antibodies were diluted in the blocking buffer and incubated with the cells for 1 hour at room temperature in a humid chamber. Samples were incubated with Hoechst in addition to the secondary antibodies to counterstain the cell nuclei. Finally, the membranes containing the stained cells were carefully removed from the permeable inserts, placed on glass slides, and mounted with VECTASHEILD mounting medium (Vector Laboratories; Burlingame, CA). Samples were imaged using a confocal microscope (Zeiss LSM 980 with Airyscan 2).

3.3.2 Transepithelial Electrical Resistance (TEER) Measurements

TEER measurements were used to indicate the presence of tight junctions formed between HCECs. Measurements were first taken after HCECs were cultured in submerged conditions for seven days followed by measurements every 2-3 days once the cells were placed at ALI. Measurements were made with the EVOM2 epithelial ohmmeter (World Precision Instruments; Sarasota, FL) at room temperature. Three measurements were recorded for each sample to get the

average resistance. A fibronectin coated permeable insert without cells kept at the same culture conditions as the samples was used as the negative control.

3.3.3 Permeability of Fluorescein Sodium

The epithelium integrity was determined by measuring the permeability of fluorescein sodium through the cell layer. 200 µL of a fluorescein sodium solution (30 µg/mL) in EpiGRO media was added to the top compartment of the permeable insert, and 600 µL of EpiGRO media was added to the bottom compartment. Samples were collected as 5 µL aliquots from both the top and bottom compartments and were separately added to wells in a 96-well plate containing 95 µL of DPBS. Between sample collections, the cells were maintained at 37°C and 5% CO_2. The fluorescent intensity (excitation 485 nm, emission 535 nm) was measured using a microplate reader (Beckman Coulter DTX 880 Multimode Detector).

The apparent permeability coefficient (P_{app}) was calculated using the following equation:

$$P_{app} = \frac{dQ}{dt} \cdot \frac{1}{A \cdot C_0 \cdot 60} \quad (1)$$

where dQ/dt is the mass flux (µg/min) of fluorescein sodium across the cell layer, A is the surface area (cm^2) of the permeable insert, C_0 is the initial concentration (µg/mL) of fluorescein sodium in the top compartment of the permeable insert at $t = 0$, and 60 is used to convert minutes to seconds such that the units of P_{app} are cm/s. Flux was obtained from the slope of the linear portion of the cumulative fluorescein sodium permeated versus time plot.

3.4 Characterization of HRMECs

3.4.1 Cell Viability

HRMECs at passage 7 were seeded in a 96-well plate coated with Attachment Factor at a seeding density of 20,000 cells/cm^2. The cells were cultured in Complete Classic media at 37°C

and 5% CO_2 until confluent (approximately 7 days) before treatment with TNF-α (10 ng/mL in Complete Classic media). Cell viability was measured before treatment with TNF-α and every 24 hours after treatment for seven days. The CellTiter-Blue assay (Promega; Madison, WI) was used to determine cell viability, and the manufacturer's protocol was followed for this analysis. Briefly, 20 μL of CellTiter-Blue reagent was added to each well containing cells in 100 μL of media. Cells were incubated at 37°C and 5% CO_2 with the reagent for 4 hours. The fluorescent intensity (excitation 560 nm, emission 590) was measured using a microplate reader (Beckman Coulter DTX 880 Multimode Detector).

3.4.2 Enzyme Linked Immunosorbent Assay (ELISA)

After treatment with TNF-α as described in Section 3.2.2, the media was collected and replaced with fresh media containing TNF-α every 24 hours for seven days. The collected media was centrifuged, and the supernatant was aliquoted and stored at -80°C until used for analysis. Commercial ELISA kits were used to detect human IL-8, IL-6, TNF-α, and IL-1β (BioLegend; San Diego, CA) according to the manufacturer's protocol. Briefly, a 96-well plate was coated with the capture antibody overnight at 4°C. The specific standards and media samples were added the following day and were incubated for 2 hours while shaking. Samples and standards were then incubated with a biotinylated detection antibody for 1 hour while shaking. Next, avidin-conjugated horse radish peroxidase was added to the plate and incubated for 30 minutes while shaking. Lastly, a TMB substrate solution added to the plate and incubated for 15 minutes. The absorbance was measured at 450 nm using a microplate reader. Four to five washes with 0.05% Tween-20 in PBS were performed between each step, and each step was performed at room temperature, unless otherwise noted.

3.4.3 Reverse Transcription Polymerase Chain Reaction (RT-PCR)

HRMECs were collected for RT-PCR after treatment with TNF-α for 24 hours by scraping the cells off the surface of the permeable inserts. Cells were lysed with TRI reagent (Molecular Research Center; Cincinnati, OH), and the manufacturer's instructions were followed to extract total RNA. 0.5 µl of glycogen (Thermo Scientific; Waltham, MA) was used as an RNA carrier, and 0.5 µg of RNA was used for reverse transcription in order to measure mRNA expression levels. RNA was treated with RNase-Free DNase I (Thermo Scientific) for 30 minutes at 37°C and subsequently reverse-transcribed into cDNA by using oligo (dT), random primers, Deoxynucleotide Triphosphates (dNTP) and Moloney Murine Leukemia Virus Reverse Transcriptase (M-MLV RT) (Thermo Scientific).

Real-time PCR was carried out in a 20-µl reaction containing specific qRT-PCR primers (Table 1) and iTaq Universal SYBR Green Supermix, (Bio-Rad Laboratories; Los Angeles, CA). PCR was performed on QuantStudio Real-Time PCR Instrument (Thermo Scientific). Cycling conditions for RT-PCR were as follows: 50°C for 2 minutes, 95°C for 10 minutes, followed by 40 cycles of 95°C for 15 seconds and 60°C for 1 minute. Each sample was performed in duplicate. β-Actin was used as the housekeeping gene. The amount of each target mRNA to the housekeeping gene was calculated using the comparative Ct method ($2^{-\Delta\Delta Ct}$) [67].

3.4.4 Immunocytochemistry

PECAM-1, VCAM-1, and ICAM-1 expression were evaluated by immunocytochemical staining. Cells were fixed and permeabilized with BD Cytofix/Cytoperm solution for 20 minutes at 4°C. Carefully, the membranes containing the cells were removed from the inserts, and the samples were blocked with 1% BSA and 0.2% (v/v) Tween-20 in DPBS for 30 minutes at room temperature. Cells were incubated with the primary or isotype control antibodies diluted in the blocking buffer overnight at 4°C in a humid chamber. Specific secondary antibodies and Hoechst, diluted in the

blocking buffer, were incubated with the cells for 1 hour at room temperature in a humid chamber. Finally, the samples were placed on glass slides and mounted with VECTASHEILD mounting medium. Samples were imaged using a confocal microscope (Zeiss LSM 980 with Airyscan 2).

Table 1. Primer sequences used in RT-PCR for HRMEC analysis.

Gene	**Forward Primer**	**Reverse Primer**
β-Actin	GCCGGGACCTGACTGACTAC	TTCTCCTTAATGTCACGCACGAT
IL-1β	TGAAGCTGATGGCCCTAAACA	GTAGTGGTGGTCGGAGATTCG
IL-6	GGTACATCCTCGACGGCATCT	GTGCCTCTTTGCTGCTTTCAC
IL-8	ACTGAGAGTGATTGAGAGTGGAC	AACCCTCTGCACCCAGTTTTC
TNF-α	CCTGCTGCACTTTGGAGTGAT	CAACATGGGCTACAGGCTTGT
PECAM1	AAGTGGAGTCCAGCCGCATATC	ATGGAGCAGGACAGGTTCAGTC
ICAM1	CAGTGGGAAAGTGCCATCCT	CTCCAATGTGCCAGGCTTG
VCAM1	CTTGCAGCTTACAGTGACAGAGC	TTCCCTAGAGATCCAGAAATCGAG

3.5 Statistical Analysis

Measurements were taken in triplicate from at least three independent experiments. Experimental results are represented as mean ± SD. Student's t-test or Tukey's multiple comparison test following an ANOVA were used to determine significance differences amongst experimental groups. A value of $p<0.05$ was considered significant. Prism (GraphPad Software; San Diego, CA) was used to perform all statistical analyses.

CHAPTER IV

RESULTS

4.1 Characterization of HCECs

4.1.1 Immunocytochemistry

HCEC morphology in the cornea module is shown in Figure 5. HCECs showed expression of CK3, and both the submerged-ALI model and the submerged model generated 3-4 layers of cells. HCECs did not have ZO-1 expression under the current protocol for either the submerged-ALI or submerged model.

4.1.2 TEER Measurements

TEER was used as one indicator for the formation of an HCEC multilayer and tight junctions between the cells (Fig. 6a). After seven days in submerged culture, the cells were exposed to ALI conditions for another seven days. At ALI, the resistance increased until Day 12, at which point it seems that the values begin to plateau. However, the cells that were maintained in submerged culture showed a gradual increase in resistance until Day 14 of culture. The cells that were maintained in submerged culture had a higher resistance at each timepoint tested than the cells that were at ALI. The final resistance measurements were $21 \pm 4\ \Omega \cdot cm^2$ and $26 \pm 5\ \Omega \cdot cm^2$ for HCECs in submerged-ALI and submerged culture, respectively.

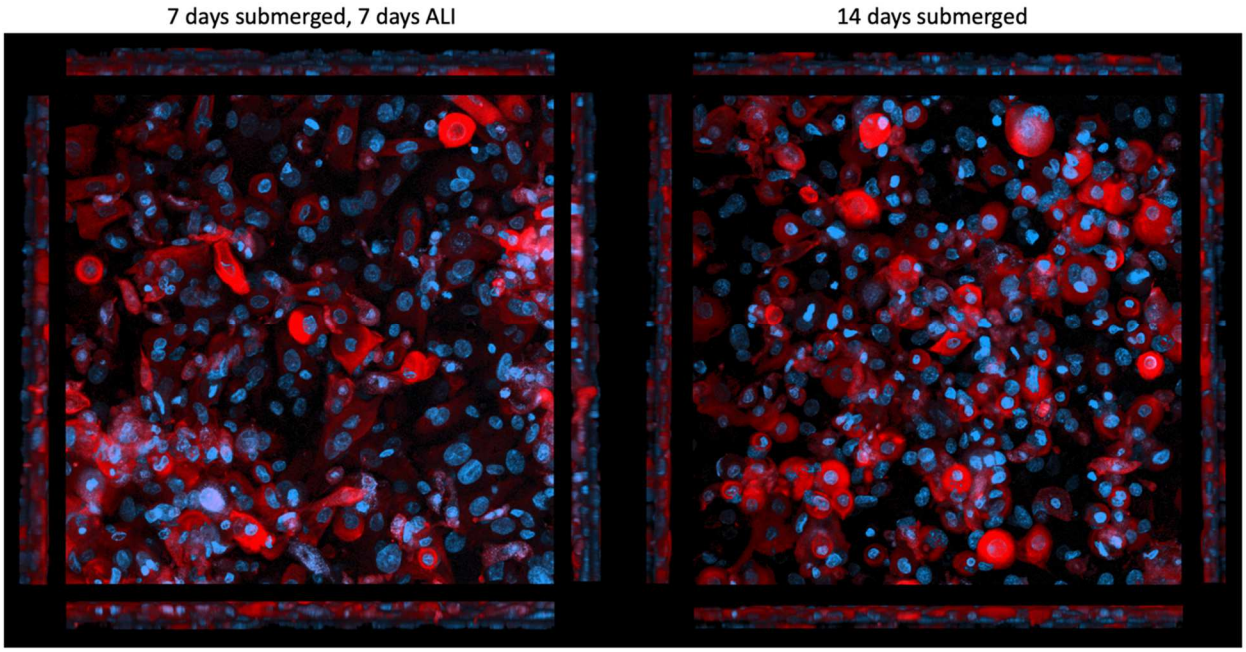

Figure 5. Cytokeratin-3 (red) expression in the cornea module. HCECs were cultured in either submerged culture followed by ALI exposure or submerged-only conditions. Nuclei were counterstained with Hoechst (blue). Side panels for each image show the cell layers present in each sample. Magnification 200x. Images are representative samples (n=3) from three independent experiments.

4.1.3 Permeability of Fluorescein Sodium

The permeability of fluorescein sodium through the HCEC layer was used as another indicator for the formation of a mature barrier within the epithelium (Fig. 6b). The apparent permeability coefficients were calculated as $(3.79 \pm 0.40) \times 10^{-3}$ cm/s for the control samples, $(2.13 \pm 0.27) \times 10^{-3}$ cm/s for the submerged-ALI samples, and $(1.66 \pm 0.24) \times 10^{-3}$ cm/s for the submerged samples. The submerged group had the lowest permeability to fluorescein sodium followed by the submerged-ALI group, and both groups with cells had significantly lower permeability than the control group which was a permeable insert coated with fibronectin.

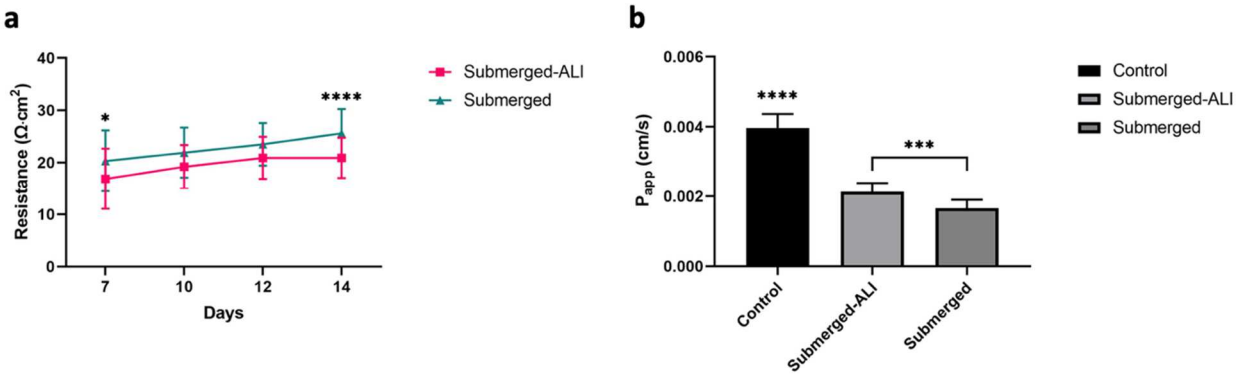

Figure 6. Barrier properties of the cornea module. (a) TEER measurements of HCECs under either submerged-ALI or submerged-only conditions. All HCECs were cultured submerged until Day 7. Background resistance of the permeable insert coated with fibronectin was subtracted from the values displayed. (b) Permeability measurements were taken on Day 14 of culture. Control samples were fibronectin-coated permeable inserts and were kept at the same culture conditions as the HCEC samples. Data shown as mean ± SD; n=3 from three independent experiments (*p<0.05; ***p<0.001; ****p<0.0001).

4.2 Characterization of HRMECs

4.2.1 ELISA

In order to determine if the HRMECs could be activated, the release of inflammatory cytokines was measured after exposure to TNF-α. The viability of HRMECs treated with TNF-α compared to untreated control HRMECs was also determined and is shown in Figure 7. The average viability over the seven-day experiment for untreated and treated cells was 95.9 ± 3.9 % and 94.4 ± 3.3 %, respectively. HRMECs showed a significant increase in IL-8 and IL-6 secretion after

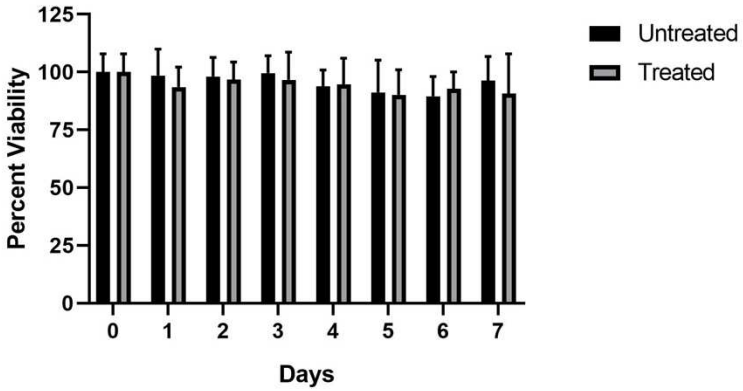

Figure 7. Percent viability of HRMECs cultured in 96-well plates. HRMECs were cultured in Complete Classic media supplemented with TNF-α (10 ng/mL) and compared to untreated control samples. Data shown as mean ± SD; n=3 from three independent experiments.

exposure to TNF-α (Fig. 8a and 8b). Concentrations of both cytokines continue to increase for the first three to four days of exposure. There were no detectable levels of TNF-α in untreated control cells, and TNF-α concentrations measured from treated cell samples were fairly consistent across all timepoints (Fig. 8c). IL-1β concentrations were only significantly higher for treated cells compared to untreated control cells after 24-hours of exposure to TNF-α (Fig. 8d). Continued exposure of treated HRMECs to TNF-α did not have a significant effect on IL-1β concentrations, which decreased significantly after 24-hours.

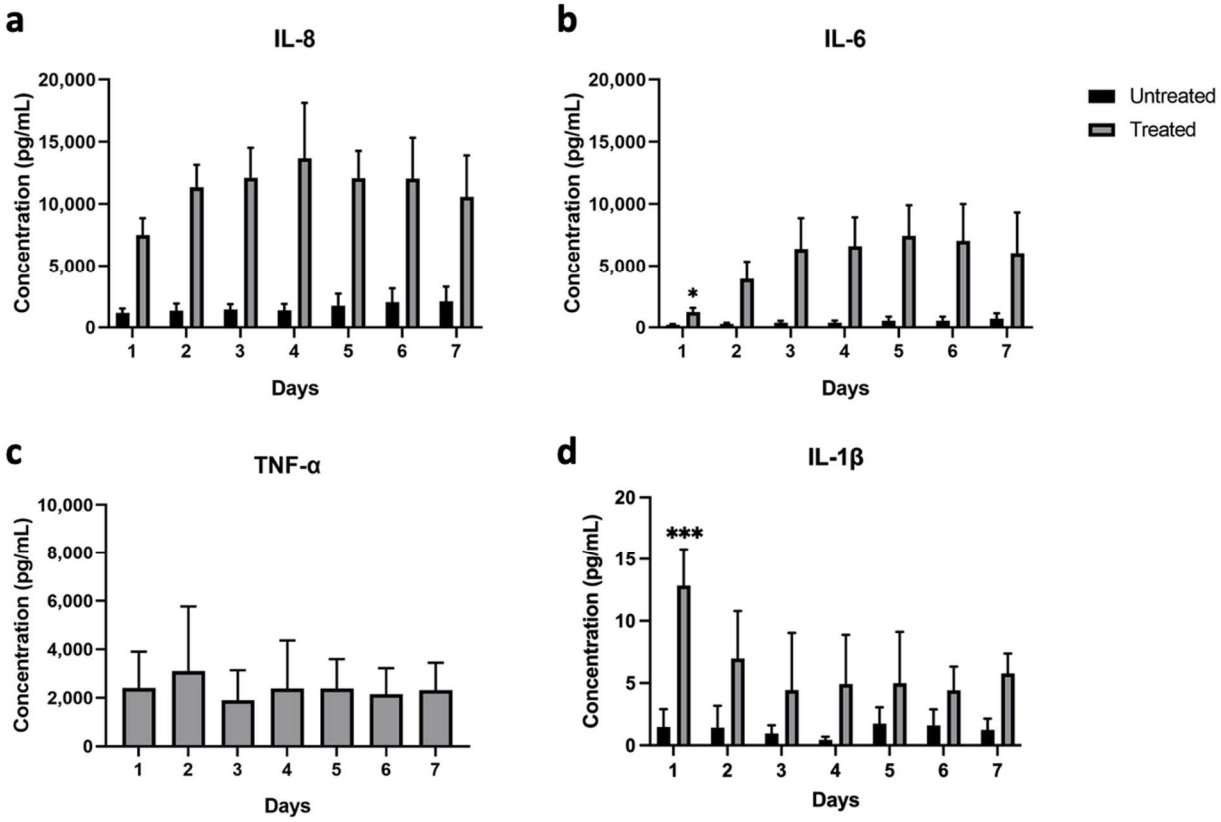

Figure 8. Cytokine concentrations from the retina module (a-c) or HRMECs cultured in 96-well plates (d). HRMECs in the module or the well plate were either untreated or treated with TNF-α (10 ng/mL). (a, b) Treated HRMECs showed significantly higher IL-8 concentrations than untreated HRMECs for all timepoints tested ($p<0.0001$) and significantly higher IL-6 concentrations than untreated HRMECs for Days 2-7 ($p<0.01$). Treated HRMECs had significantly higher IL-6 concentrations on Days 2-7 compared to Day 1 (*$p<0.05$). (c) There were no detectable levels of TNF-α from untreated HRMECs for the timepoints measured. (d) Treated HRMECs had significantly higher IL-1β concentrations on Day 1 compared to Days 3-7 and to untreated HRMECs for all timepoints tested (**$p<0.01$). Data shown as mean ± SD; n=3 from three independent experiments.

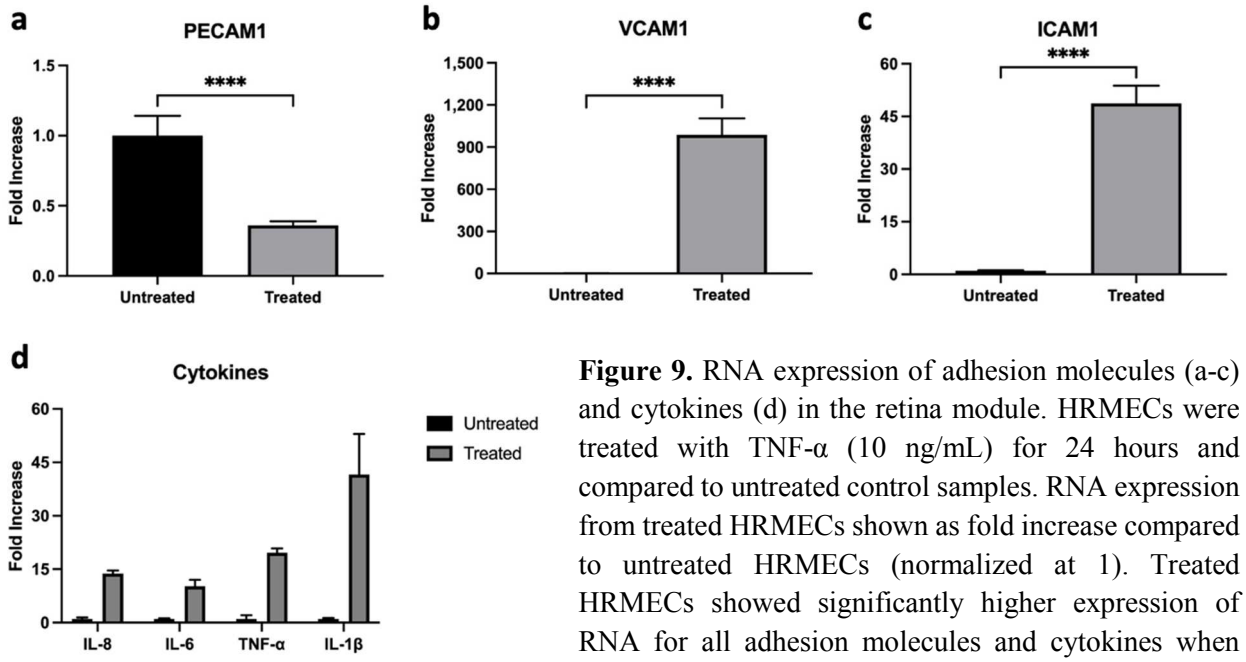

Figure 9. RNA expression of adhesion molecules (a-c) and cytokines (d) in the retina module. HRMECs were treated with TNF-α (10 ng/mL) for 24 hours and compared to untreated control samples. RNA expression from treated HRMECs shown as fold increase compared to untreated HRMECs (normalized at 1). Treated HRMECs showed significantly higher expression of RNA for all adhesion molecules and cytokines when compared to untreated HRMECs ($p<0.0001$). Data shown as mean ± SD; n=3 from three independent experiments.

4.2.2 RT-PCR

RNA expression of inflammatory cellular adhesion molecules and cytokines was also evaluated after TNF-α exposure to determine the activation state of the HRMECs. Baseline expression of PECAM1 was significantly higher than baseline expression of VCAM1 and ICAM1 (Appendix A). After treatment with TNF-α, PECAM1 expression decreased approximately 0.4-fold (Fig. 9a), but VCAM1 and ICAM1 expression increased 988-fold and 49-fold, respectively (Fig. 9b and 9c). Additionally, all four inflammatory cytokines measured showed significant increases in expression (at least 10-fold) after treatment with TNF-α when compared to the untreated control (Fig. 9d).

4.2.3 Immunocytochemistry

HRMEC morphology in the retina module before and after treatment with TNF-α is shown in Figure 10. HRMECs showed expression of PECAM-1 and have an even distribution in the cell

layer. Additionally, cell density is unaffected by exposure to TNF-α. Untreated cells showed little to no expression of ICAM-1 and VCAM-1. After treatment with TNF-α, the HRMECs have a high expression of ICAM-1 and a moderate expression of VCAM-1.

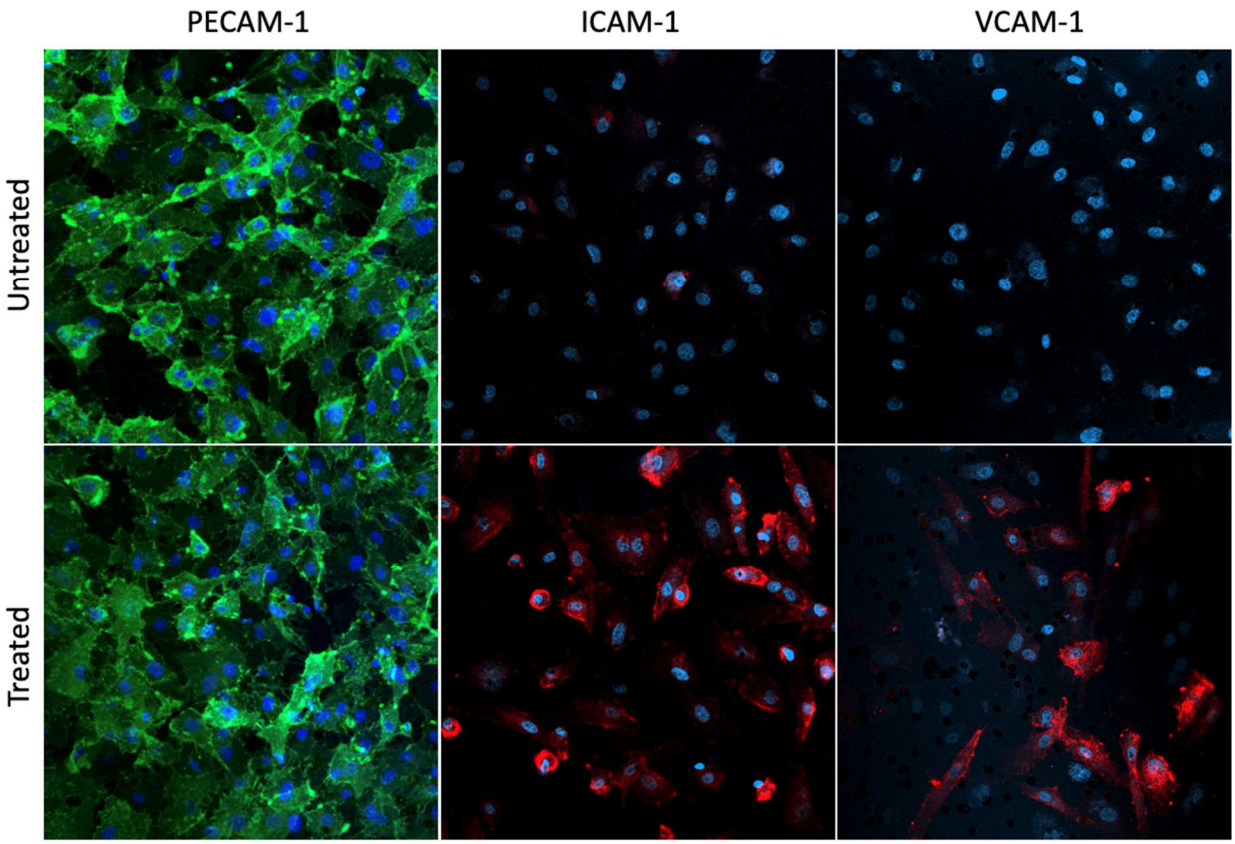

Figure 10. PECAM-1 (green), ICAM-1 (red), and VCAM-1 (red) expression in the retina model. HRMECs were treated with TNF-α (10 ng/mL) for 24 hours and compared to untreated control samples. Cells were counterstained with Hoechst (blue). Magnification 200x. Images are representative samples from three independent experiments.

CHAPTER V

DISCUSSION AND CONCLUSIONS

5.1 Discussion

The drug delivery system developed by our lab [9] aims to treat diabetic retinopathy by topical application to the eye. Therefore, our model to test this system must have two important functions. First, the model must include a barrier component that mimics how the cornea will interact with the drug delivery system. A mature corneal epithelium contains multiple cell layers and contains tight junctions in the outermost cell layer and culturing *in vitro* models at ALI helps to develop this mature epithelium. Our model formed multiple cell layers; however, additional layers were not formed after culturing at ALI, which was expected [51]. Our model contained four cell layers, which is comparable to other models that generate a minimum of four [56, 57, 62] or five [51, 61] cell layers after culturing at ALI.

Even though there was no tight junction protein (i.e., ZO-1) expression detected in the model, TEER measurements and the apparent permeability coefficient of fluorescein sodium suggest the presence of tight junctions. Our model produced resistances significantly higher and P_{app} values significantly lower than the control samples; however, the values differed from those reported in literature. It has been noted that TEER values greater than 200 $\Omega \cdot cm^2$ indicate a mature corneal barrier [61]. *In vitro* models using cell lines obtain TEER values ranging from 200 $\Omega \cdot cm^2$ to over 1000 $\Omega \cdot cm^2$ [51, 55-58]. Models using primary cells have reported TEER values ranging from approximately 870-1,1400 $\Omega \cdot cm^2$ [61, 62]. However, these primary cell models were cultured

on permeable inserts with 0.4 μm diameter pores, which is an order of magnitude smaller than the pore size used in our model. Primary cell models cultured on membranes with 3.0 μm pores have reported TEER values less than 100 $\Omega \cdot cm^2$ [55], which is similar to our models cultured on membranes with 8.0 μm pores. It has been suggested smaller pore sizes are best for growing multiple layers of HCECs compared to larger pores because cell migration through the membrane is prevented [51]. However, this may not always true. One study showed that the cell migration through membranes with 3.0 μm pores could create a dual epithelial layer to provide greater resistance than a multilayer on membranes with 0.4 μm pores [54].

Studies have shown the resistance of the epithelium can be increased by changing the culture conditions. In one model using a cell line, TEER values were increased from 69-113 $\Omega \cdot cm^2$ to approximately 500 $\Omega \cdot cm^2$ by leaving a thin liquid layer on the cells at ALI to mimic the tear film and re-submerging the model after ALI culture. Another study using rabbit cells was able to significantly increase the resistance of the cell layer from 22 $\Omega \cdot cm^2$ to 72 $\Omega \cdot cm^2$ by exposing the model to culture conditions, termed dynamic ALI, that continuously alternates between submerged and ALI culture conditions [68].

When considering P_{app} of our model, the permeability values for both culture conditions are much higher than other reported values for *in vitro* models. Other studies that report fluorescein sodium P_{app} for *in vitro* cornea models are all on the order of 10^{-7} cm/s, ranging from approximately 1.4-7.0 $x10^{-7}$ cm/s [56, 57, 61, 62], and are comparable to permeability coefficients for fluorescein sodium in excised rabbit (~3.8 $x10^{-7}$ cm/s [57, 61]) and porcine (1.5-1.8 $x10^{-7}$ cm/s [54, 57]) corneas. Most of these *in vitro* models are cultured on membranes with 0.4 μm pores. Although these membranes were likely used to promote the formation of tight epithelial layers, they may have also acted as a barrier to the permeation of fluorescein sodium. We did not want the membrane to act as a barrier for drug delivery, which is why we used permeable membrane inserts with 8.0 μm pores. The one *in vitro* model [57] that was cultured on a membrane with 3.0 μm pores had an

additional component not seen in the other models; the corneal epithelial cells were cultured on a collagen matrix containing keratocytes, which was intended to represent the stroma. This stromal layer was shown to affect permeability of fluorescein sodium based on its thickness, which shows it is an additional barrier to permeation.

Second, the model must include the cell type that is the target for treatment, and the cell type must be able to replicate the functionality seen under the disease conditions. We intend to use the model to study treatment options for diabetic retinopathy. Therefore, retinal microvascular endothelial cells in an inflamed state are an essential component for this model. Some retina models have reported a decrease in viability after exposure to TNF-α for 24 [69] or 48 hours [70], but the viability of cells in our model is not affected after seven days of exposure. There is a significant increase in secretion of IL-8 and IL-6 after activation, which mimics the concentration increase of IL-8 and IL-6 in the vitreous of patients with DR when compared to patients without DR [34, 35, 71-73]. The increased gene expression of IL-8 and IL-6 in our model was similar to the reported 5- to 21-fold increase in IL-8 gene expression [38, 70] and 4.5- to 5.5-fold increase in IL-6 gene expression [70, 74].

TNF-α and IL-1β are also known to increase in the vitreous in DR patients [34-37], but these cytokines are known to be released by activated microglial cells in the retina. In the model, although the HRMECs showed increased IL-1β secretion, it was only significantly increased within the first 24 hours of exposure to TNF-α. The gene expression was also significantly increased during this same window of time, but the trends in gene expression after 24 hours were not measured. There was an increase in gene expression for TNF-α during the first 24 hours, but the measured concentrations of TNF-α from treated HRMECs seemed somewhat consistent during the seven-day experiment. Since TNF-α was used to activate the cells, the measured TNF-α from the treated HRMECs shows the cytokine remaining after uptake by the cells. The slight increase in TNF-α concentrations on Day 2 may be a result of delayed cytokine uptake, but this increase was

not significant. Based on these results, HRMECs may produce very low levels of TNF-α and IL-1β in the retina, but they are insignificant when compared to cytokine production of other cells present. TNF-α and IL-1β are used in *in vitro* models to activate cells to an inflammatory state. Both TNF-α and IL-1β indirectly trigger the inflammatory response by inducing expression of other inflammatory cytokines, such as IL-6 and IL-8 [45, 46]. Sustained expression of these cytokines at elevated levels in the retina prolongs inflammation by the continual recruitment of leukocytes. DR may worsen over time if the levels of proinflammatory cytokines remained elevated and the inflammatory response is unable to be resolved.

TNF-α and IL-1β also induce expression of cell adhesion molecules such as VCAM-1 and ICAM-1 [45, 47]. This was seen in our model. Both the protein expression and the gene expression of VCAM-1 and ICAM-1 were upregulated after exposure to TNF-α. Others have shown increases of these adhesion molecules in HRMECs too [70, 75]. PECAM-1 gene expression was downregulated in our model after exposure to TNF-α for 24 hours, as seen with human umbilical vein endothelial cells (HUVECs) [76]. However, the protein expression for PECAM-1 was unchanged . Studies have also reported no change in PECAM-1 protein expression in HUVECs [76] and human skin grafts [77] after treatment with TNF-α 24 hours, although protein expression may require two to three days after treatment to be altered [78]. PECAM-1 has been identified as a player in leukocyte transendothelial migration [79]; therefore, the cell may downregulate this gene to counteract the increased permeability to leukocytes caused by TNF-α.

5.2 Conclusions

The project aim was to create an eye model that can be used to test drug delivery systems for the treatment of retinal diseases has resulted in a two-module system that represents the cornea, the main barrier to topical drug delivery, and the retinal vascular system, the target for pharmacotherapy when treating diabetic retinopathy. The retinal module was successfully activated

by TNF-α. The HRMECs expressed VCAM-1 and ICAM-1, cellular markers of inflammation, after treatment with the activating agent. The cells also had increased gene expression and secretion of inflammatory cytokines IL-8 and IL-6. IL-1β and TNF-α may also be secreted, but the contribution of HRMECs to these cytokine levels in the retina may be insignificant when compared to secretion by other cells in the retina that are activated under conditions characteristic of DR.

The cornea module shows multiple cell layers that can provide a barrier to drug transport; however, further development is needed to represent an *in vivo* cornea. While our model did display a multilayer of HCECs, these cells may not be a fully mature epithelium as evidenced by the lack of tight junction protein (i.e., ZO-1) expression. Additionally, the epithelial resistance was lower and the permeability was higher than those reported for other *in vitro* cornea models.

Overall, the two-module eye model created here is the first step towards an eye model that can be used as a preclinical tool to study drug delivery to the posterior of the eye. With the development of a tissue-engineered eye model to test drug delivery, new drugs can quickly easily be tested for their efficacy in treating DR and preventing blindness.

5.3 Future Directions

Future work on this eye model should be focused on the cornea module. A mature multilayer should be formed in order for the module to give better predictions for drug transport from a topical drug delivery system. Based on the results presented above, the submerged model had better barrier properties than the submerged-ALI model. This may indicate the HCECs have not reach confluency after only seven days of submerged culture. Therefore, increasing the amount of time the model is cultured at submerged conditions before exposure to ALI may help to form a tighter HCEC monolayer. Alternately, increasing the initial cell seeding density may allow the formation of this tight monolayer during the same seven-day timespan in submerged culture conditions that was used for the model discussed above. Alternatively, the HCECs could possibly

be induced to form tight junction proteins. As previously mentioned, the corneal epithelium is a stratified squamous multilayer, and the cells differentiate to form the basal, wing, and superficial cells found in the multilayer. Various pathways and transcription factors that initiate differentiation of HCECs into these different cell types have been investigated [80]. Using this knowledge, culture conditions could be modified to promote differentiation and formation of tight junctions. Once the barrier properties are improved in the cornea module, testing the drug delivery system may begin.

Future work for the retina module may include studying the effect of inflammation on the barrier properties of the HRMECs. An undamaged retinal endothelium displays tight junctions that form the blood-retinal barrier. Upon inflammation, endothelial cells become damaged, which may result in a leaky barrier. TEER measurements can be used to test the change in barrier properties after exposure to TNF-α.

REFERENCES

1. Cheung, N., P. Mitchell, and T.Y. Wong, *Diabetic retinopathy.* Lancet, 2010. **376**(9735): p. 124-36.

2. Kolb, H., *How the Retina Works: Much of the construction of an image takes place in the retina itself through the use of specialized neural circuits.* American Scientist, 2003. **91**(1): p. 28-35.

3. Steinmetz, J.D., et al., *Causes of blindness and vision impairment in 2020 and trends over 30 years, and prevalence of avoidable blindness in relation to VISION 2020: the Right to Sight: an analysis for the Global Burden of Disease Study.* The Lancet Global Health, 2021. **9**(2): p. e144-e160.

4. Boyd, K. and G.A. Vemulakonda. *What Is Diabetic Retinopathy?* October 24, 2019; Available from: https://www.aao.org/eye-health/diseases/what-is-diabetic-retinopathy.

5. *Macular Degeneration Treatments*. Available from: https://www.macular.org/treatments.

6. *Glaucoma*. July 28, 2020; Available from: https://www.nei.nih.gov/learn-about-eye-health/eye-conditions-and-diseases/glaucoma.

7. Kompella, U.B., et al., *Nanomedicines for back of the eye drug delivery, gene delivery, and imaging.* Progress in Retinal and Eye Research, 2013. **36**: p. 172-198.

8. Bisht, R., et al., *Nanocarrier mediated retinal drug delivery: overcoming ocular barriers to treat posterior eye diseases.* Wiley Interdiscip. Rev.: Nanomed. Nanobiotechnol., 2018. **10**(2): p. n/a.

9. Sharma, M., R. Bhowmick, and H. Gappa-Fahlenkamp, *Drug-Loaded Nanoparticles Embedded in a Biomembrane Provide a Dual-Release Mechanism for Drug Delivery to the Eye.* J Ocul Pharmacol Ther, 2016. **32**(9): p. 565-573.

10. Sridhar, M.S., *Anatomy of cornea and ocular surface.* Indian journal of ophthalmology, 2018. **66**(2): p. 190-194.

11. Wilson, S.E., *Bowman's layer in the cornea– structure and function and regeneration.* Experimental Eye Research, 2020. **195**: p. 108033.

12. Feng, K., C. You, and L. Yuan, *General Anatomy*, in *Anatomy and Examination in Ocular Trauma*, H. Yan, Editor. 2019, Springer Singapore: Singapore. p. 3-30.

13. de Oliveira, R.C. and S.E. Wilson, *Descemet's membrane development, structure, function and regeneration.* Experimental Eye Research, 2020. **197**: p. 108090.

14. Kolb, H., *Simple Anatomy of the Retina.* Webvision: The Organization of the Retina and Visual System, 2011.

15. Boyd, K. and N.Z. Gregori. *What Is Macular Degeneration?* January 26, 2021; Available from: https://www.aao.org/eye-health/diseases/amd-macular-degeneration.

16. Cousins, S.W., K.G. Csaky, and D.G. Espinosa-Heidmann, *Clinical Strategies for Diagnosis and Treatment of AMD: Implications from Research*, in *Macular Degeneration*, P.L. Penfold and J.M. Provis, Editors. 2005, Springer Berlin Heidelberg: Berlin, Heidelberg. p. 167-200.

17. Hageman, G.S., et al., *Age-Related Macular Degeneration (AMD).*

18. Boyd, K. and J.K. McKinney. *What Is Glaucoma?* June 15, 2021; Available from: https://www.aao.org/eye-health/diseases/what-is-glaucoma.

19. Križaj, D., *What is glaucoma?* Webvision: The Organization of the Retina and Visual System [Internet], 2019.

20. Ansari, W. and S. Sharma, *Diabetic Eye Diseases*, in *Vitreoretinal Disorders*, G. Yiu, Editor. 2018, Springer Singapore: Singapore. p. 71-89.

21. Meyerle, C.B., E.Y. Chew, and F.L. Ferris, *Nonproliferative Diabetic Retinopathy*, in *Diabetic Retinopathy*, E.J. Duh, Editor. 2008, Humana Press: Totowa, NJ. p. 3-27.

22. Joussen, A.M., et al., *A central role for inflammation in the pathogenesis of diabetic retinopathy.* The FASEB Journal, 2004. **18**(12): p. 1450-1452.

23. Abiko, T., et al., *Characterization of Retinal Leukostasis and Hemodynamics in Insulin Resistance and Diabetes.* Diabetes, 2003. **52**(3): p. 829.

24. Miyamoto, K., et al., *Prevention of leukostasis and vascular leakage in streptozotocin-induced diabetic retinopathy via intercellular adhesion molecule-1 inhibition.* Proceedings of the National Academy of Sciences, 1999. **96**(19): p. 10836.

25. Joussen, A.M., et al., *Leukocyte-Mediated Endothelial Cell Injury and Death in the Diabetic Retina.* The American Journal of Pathology, 2001. **158**(1): p. 147-152.

26. Adamis, A., *Is diabetic retinopathy an inflammatory disease?* 2002, BMJ Publishing Group Ltd.

27. Aiello, L.P., et al., *Vascular Endothelial Growth Factor in Ocular Fluid of Patients with Diabetic Retinopathy and Other Retinal Disorders.* New England Journal of Medicine, 1994. **331**(22): p. 1480-1487.

28. Forrester, J.V., L. Kuffova, and M. Delibegovic, *The Role of Inflammation in Diabetic Retinopathy.* Frontiers in Immunology, 2020. **11**(2644).

29. Yoshida, S., A. Yoshida, and T. Ishibashi, *Induction of IL-8, MCP-1, and bFGF by TNF-α in retinal glial cells: implications for retinal neovascularization during post-ischemic*

inflammation. Graefe's Archive for Clinical and Experimental Ophthalmology, 2004. **242**(5): p. 409-413.

30. Chan, C.K., et al., *Differential expression of pro- and antiangiogenic factors in mouse strain-dependent hypoxia-induced retinal neovascularization.* Laboratory Investigation, 2005. **85**(6): p. 721-733.

31. Yoshida, S., et al., *Involvement of interleukin-8, vascular endothelial growth factor, and basic fibroblast growth factor in tumor necrosis factor alpha-dependent angiogenesis.* Molecular and cellular biology, 1997. **17**(7): p. 4015-4023.

32. Nehmé, A. and J. Edelman, *Dexamethasone Inhibits High Glucose–, TNF-α–, and IL-1β–Induced Secretion of Inflammatory and Angiogenic Mediators from Retinal Microvascular Pericytes.* Investigative Ophthalmology & Visual Science, 2008. **49**(5): p. 2030-2038.

33. Busik, J.V., S. Mohr, and M.B. Grant, *Hyperglycemia-induced reactive oxygen species toxicity to endothelial cells is dependent on paracrine mediators.* Diabetes, 2008. **57**(7): p. 1952-1965.

34. Tang, J. and T.S. Kern, *Inflammation in diabetic retinopathy.* Progress in Retinal and Eye Research, 2011. **30**(5): p. 343-358.

35. Yuuki, T., et al., *Inflammatory cytokines in vitreous fluid and serum of patients with diabetic vitreoretinopathy.* Journal of Diabetes and its Complications, 2001. **15**(5): p. 257-259.

36. Shanmuganathan, S. and N. Angayarkanni, *Chebulagic acid Chebulinic acid and Gallic acid, the active principles of Triphala, inhibit TNFα induced pro-angiogenic and pro-inflammatory activities in retinal capillary endothelial cells by inhibiting p38, ERK and NFkB phosphorylation.* Vascul Pharmacol, 2018. **108**: p. 23-35.

37. Ben-Mahmud, B.M., et al., *Tumor necrosis factor-α in diabetic plasma increases the activity of core 2 GlcNAc-T and adherence of human leukocytes to retinal endothelial cells: significance of core 2 GlcNAc-T in diabetic retinopathy.* Diabetes, 2004. **53**(11): p. 2968-2976.

38. Crane, I.J., et al., *Control of chemokine production at the blood-retina barrier.* Immunology, 2000. **101**(3): p. 426-33.

39. Abu El-Asrar, A.M., et al., *Myofibroblasts in proliferative diabetic retinopathy can originate from infiltrating fibrocytes and through endothelial-to-mesenchymal transition (EndoMT).* Experimental Eye Research, 2015. **132**: p. 179-189.

40. Hirano, T., *Interleukin-6*, in *The Cytokine Handbook*, A. Thomson, Editor. 1998, Academic Press. p. 197-228.

41. Mantovani, A. and E. Dejana, *Functional Responses Elicited in Endothelial Cells by Cytokines*, in *Cytokines in Health and Disease*, S.L. Kunkel and D.G. Remick, Editors. 1992, Marcel Dekker, Inc. p. 297-307.

42. Cox, G. and J. Gauldie, *Structure and Function of Interleukin-6*, in *Cytokines in Health and Disease*, S.L. Kunkel and D.G. Remick, Editors. 1992, Marcel Dekker, Inc. p. 97-120.

43. Scales, W.E., *Structure and Function of Interleukin-1*, in *Cytokines in Health and Disease*, S.L. Kunkel and D.G. Remick, Editors. 1992, Marcel Dekker, Inc. p. 15-26.

44. Wuyts, A., P. Proost, and J. Van Damme, *Interleukin-8 and Other CXC Chemokines*, in *The Cytokine Handbook*, A. Thomson, Editor. 1998, Academic Press. p. 271-311.

45. Moldawer, L.L., *The Beneficial Role of Cytokines, Particularly Interleukin-1, in the Host Response to Injury, Infection, and Inflammation*, in *Cytokines in Health and Disease*, S.L. Kunkel and D.G. Remick, Editors. 1992, Marcel Dekker, Inc. p. 217-234.

46. Tsuji, Y. and F.M. Torti, *Tumor Necrosis Factor: Structure and Function*, in *Cytokines in Health and Disease*, S.L. Kunkel and D.G. Remick, Editors. 1992, Marcel Dekker, Inc. p. 131-150.

47. Zhang, M. and K.J. Tracey, *Tumor Necrosis Factor*, in *The Cytokine Handbook*, A. Thomson, Editor. 1998, Academic Press. p. 517-548.

48. Boyd, K. and N.Z. Gregori. *What is Vitrectomy?* April 22, 2021; Available from: https://www.aao.org/eye-health/treatments/what-is-vitrectomy.

49. Wang, W. and A.C.Y. Lo, *Diabetic Retinopathy: Pathophysiology and Treatments.* International Journal of Molecular Sciences, 2018. **19**(6): p. 1816.

50. Bandello, F., et al., *Pathophysiology and treatment of diabetic retinopathy.* Acta Diabetologica, 2013. **50**(1): p. 1-20.

51. Toropainen, E., et al., *Culture model of human corneal epithelium for prediction of ocular drug absorption.* Invest Ophthalmol Vis Sci, 2001. **42**(12): p. 2942-2948.

52. Chang, J.-E., S.K. Basu, and V.H. Lee, *Air-interface condition promotes the formation of tight corneal epithelial cell layers for drug transport studies.* Pharmaceutical research, 2000. **17**(6): p. 670-676.

53. Zieske, J.D., et al., *Basement Membrane Assembly and Differentiation of Cultured Corneal Cells: Importance of Culture Environment and Endothelial Cell Interaction.* Experimental Cell Research, 1994. **214**(2): p. 621-633.

54. Juretic, M., et al., *HCE-T cell-based permeability model: A well-maintained or a highly variable barrier phenotype?* Eur. J. Pharm. Sci., 2017. **104**: p. 23-30.

55. Reichl, S., *Cell culture models of the human cornea - a comparative evaluation of their usefulness to determine ocular drug absorption in-vitro.* J. Pharm. Pharmacol., 2008. **60**(3): p. 299-307.

56. Becker, U., et al., *A comparative evaluation of corneal epithelial cell cultures for assessing ocular permeability.* ATLA, Altern. Lab. Anim., 2008. **36**(1): p. 33-44.

57. Hahne, M. and S. Reichl, *Development of a serum-free human cornea construct for in vitro drug absorption studies: The influence of varying cultivation parameters on barrier characteristics.* International Journal of Pharmaceutics, 2011. **416**(1): p. 268-279.

58. Tanaka, H., et al., *Rebamipide increases barrier function and attenuates TNFα-induced barrier disruption and cytokine expression in human corneal epithelial cells.* Br J Ophthalmol, 2013. **97**(7): p. 912-916.

59. Araki-Sasaki, K., et al., *An SV40-immortalized human corneal epithelial cell line and its characterization.* Investigative ophthalmology & visual science, 1995. **36**(3): p. 614-621.

60. Hahne, M., et al., *Prevalidation of a human cornea construct as an alternative to animal corneas for in vitro drug absorption studies.* J. Pharm. Sci., 2012. **101**(8): p. 2976-2988.

61. Kaluzhny, Y., et al., *New Human Organotypic Corneal Tissue Model for Ophthalmic Drug Delivery Studies.* Invest Ophthalmol Vis Sci, 2018. **59**(7): p. 2880-2898.

62. Chacon, M., et al., *QobuR - A new in vitro human corneal epithelial model for preclinical drug screening.* Eur. J. Pharm. Biopharm., 2019. **136**: p. 164-173.

63. Inada, M., et al., *Microglia increase tight-junction permeability in coordination with Muller cells under hypoxic condition in an in vitro model of inner blood-retinal barrier.* Exp. Eye Res., 2021. **205**: p. 108490.

64. Fresta, C.G., et al., *A new human Blood-retinal barrier model based on endothelial cells, pericytes, and astrocytes.* Int. J. Mol. Sci., 2020. **21**(5): p. 1636.

65. Mazzeo, A., et al., *Effects of thiamine and fenofibrate on high glucose and hypoxia-induced damage in cell models of the inner blood-retinal barrier.* Acta Diabetol., 2020. **57**(12): p. 1423-1433.

66. Eyre, J.J., R.L. Williams, and H.J. Levis, *A human retinal microvascular endothelial-pericyte co-culture model to study diabetic retinopathy in vitro.* Exp. Eye Res., 2020. **201**: p. 108293.

67. Schmittgen, T.D. and K.J. Livak, *Analyzing real-time PCR data by the comparative CT method.* Nature protocols, 2008. **3**(6): p. 1101-1108.

68. Wu, Z., et al., *Reconstruction of auto-tissue-engineered lamellar cornea by dynamic culture for transplantation: a rabbit model.* PLoS One, 2014. **9**(4): p. e93012.

69. Aveleira, C.A., et al., *TNF-α Signals Through PKCζ/NF-κB to Alter the Tight Junction Complex and Increase Retinal Endothelial Cell Permeability.* Diabetes, 2010. **59**(11): p. 2872.

70. Li, H., et al., *Vascular protection of DPP-4 inhibitors in retinal endothelial cells in in vitro culture.* Int. Immunopharmacol., 2019. **66**: p. 162-168.

71. Canataroglu, H., et al., *Interleukin (IL)-6, interleukin (IL)-8 levels and cellular composition of the vitreous humor in proliferative diabetic retinopathy, proliferative vitreoretinopathy, and traumatic proliferative vitreoretinopathy.* Ocular Immunology & Inflammation, 2005. **13**(5): p. 375-381.

72. Suzuki, Y., et al., *Expression profiles of cytokines and chemokines in vitreous fluid in diabetic retinopathy and central retinal vein occlusion.* Japanese journal of ophthalmology, 2011. **55**(3): p. 256-263.

73. Hernandez, C., et al., *Interleukin□8, monocyte chemoattractant protein□1 and IL□10 in the vitreous fluid of patients with proliferative diabetic retinopathy.* Diabetic Medicine, 2005. **22**(6): p. 719-722.

74. Bogdanov, P., et al., *Calcium dobesilate prevents the oxidative stress and inflammation induced by diabetes in the retina of db/db mice.* J Diabetes Complications, 2017. **31**(10): p. 1481-1490.

75. Nehme, A. and J. Edelman, *Dexamethasone inhibits high glucose-, TNF-alpha-, and IL-1beta-induced secretion of inflammatory and angiogenic mediators from retinal microvascular pericytes.* Invest Ophthalmol Vis Sci, 2008. **49**(5): p. 2030-8.

76. Sawa, Y., et al., *Effects of TNF-α on Leukocyte Adhesion Molecule Expressions in Cultured Human Lymphatic Endothelium.* Journal of Histochemistry & Cytochemistry, 2007. **55**(7): p. 721-733.

77. Yan, H.-C., et al., *Human/severe combined immunodeficient mouse chimeras. An experimental in vivo model system to study the regulation of human endothelial cell-leukocyte adhesion molecules.* The Journal of clinical investigation, 1993. **91**(3): p. 986-996.

78. Goldberger, A., et al., *Biosynthesis and processing of the cell adhesion molecule PECAM-1 includes production of a soluble form.* Journal of Biological Chemistry, 1994. **269**(25): p. 17183-17191.

79. Newman, P.J., *The biology of PECAM-1.* The Journal of clinical investigation, 1997. **99**(1): p. 3-8.

80. Ortiz-Melo, M.T., et al., *Transcriptional profiles along cell programming into corneal epithelial differentiation.* Experimental Eye Research, 2021. **202**: p. 108302.

APPENDICES

Appendix A: Relative Gene Expression

Gene expression of adhesion molecules and cytokines relative to β-actin is shown below in Figure 11. Baseline expression of PECAM1 was significantly higher than the baseline expression of VCAM1 and ICAM1 ($p<0.0001$). After treatment with TNF-α, PECAM1 expression significantly decreased, and expression of VCAM1 and ICAM1 significantly increased. Gene expression of the four cytokines measured also significantly increased after exposure to TNF-α.

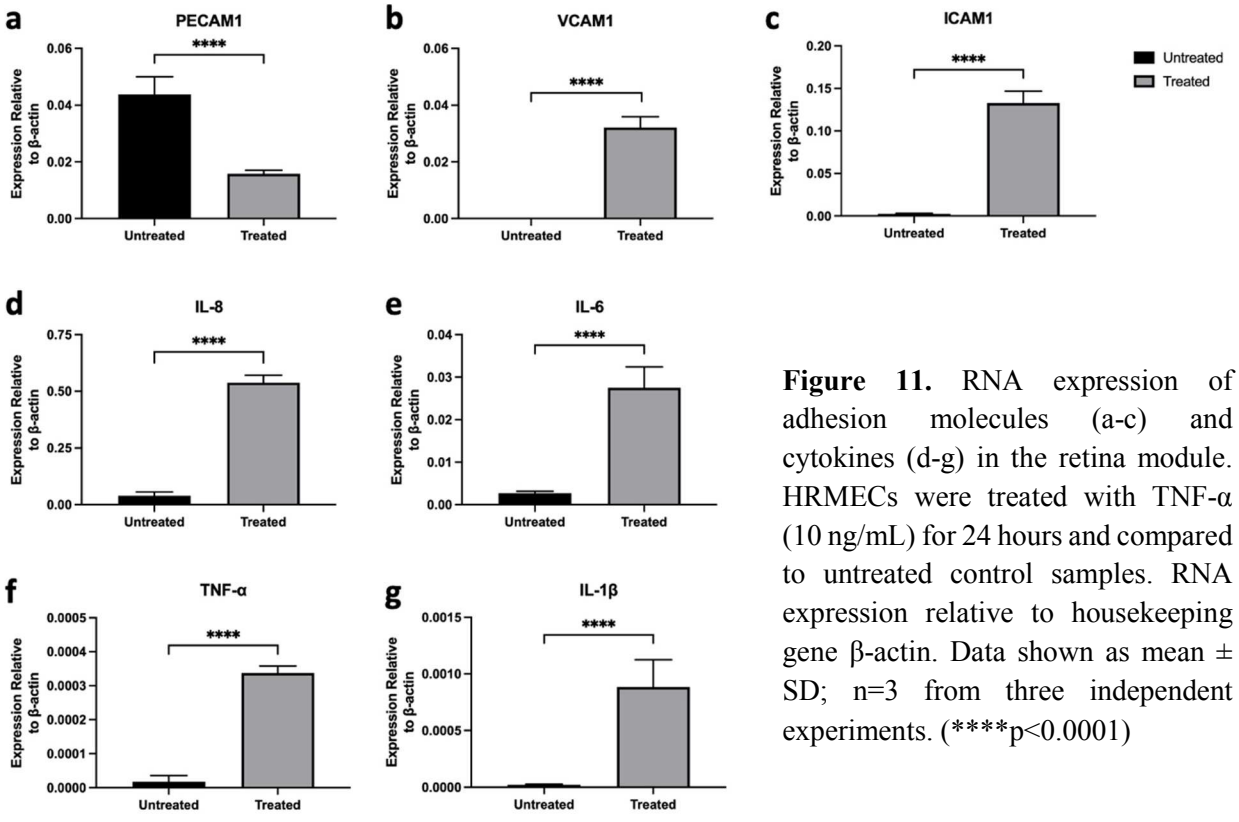

Figure 11. RNA expression of adhesion molecules (a-c) and cytokines (d-g) in the retina module. HRMECs were treated with TNF-α (10 ng/mL) for 24 hours and compared to untreated control samples. RNA expression relative to housekeeping gene β-actin. Data shown as mean ± SD; n=3 from three independent experiments. (****$p<0.0001$)

VITA

Katie Jane Oswalt

Candidate for the Degree of

Master of Science

Thesis: DEVELOPMENT OF A TISSUE-ENGINEERED EYE MODEL TO TEST DRUG DELIVERY SYSTEMS

Major Field: Chemical Engineering

Biographical:

Education:

Completed the requirements for the Master of Science in Chemical Engineering at Oklahoma State University, Stillwater, Oklahoma in December 2021.

Completed the requirements for the Bachelor of Science in Chemical and Biological Engineering at the University of Colorado Boulder, Boulder, Colorado in May 2018.

Experience:

Graduate Research Assistant, Oklahoma State University, Department of Chemical Engineering, August 2018 – December 2021

Undergraduate Research Assistant, University of Colorado Boulder, Department of Chemical and Biological Engineering, January 2017 – October 2017

Professional Memberships:

Biomedical Engineering Society (BMES)
American Institute of Chemical Engineers (AIChE)
Tau Beta Pi Engineering Honor Society
Society of Women Engineers (SWE)